Drought variation of western Chinese Loess Plateau since 1568 and its linkages

with droughts in western North America

Keyan Fang[1,2,3*], Zhengtang Guo[3,4], Deliang Chen[2], Hans W. Linderholm[2], Jinbao Li[5],

Feifei Zhou[1], Guoyang Guo[1], Zhipeng Dong[1], Yingjun Li[1]

1. Institute of Geography, Key Laboratory of Humid Subtropical Eco-geographical Process (Ministry of Education), College of Geographical Sciences, Fujian Normal University, Fuzhou 350007, China

2. Regional Climate Group, Department of Earth Sciences, University of Gothenburg, Box 460 S-405 30 Gothenburg, Sweden

3. Key Laboratory of Cenozoic Geology and Environment, Institute of Geology and Geophysics, Chinese Academy of Sciences, Beijing 100029, China

4. CAS Center for Excellence in Tibetan Plateau Earth Sciences

5. Department of Geography, University of Hong Kong, Pokfulam, Hong Kong.

[*] To whom correspondence should be addressed: Email: kfang@fjnu.edu.cn

23

Abstract

Understanding long-term drought variations in the past can help to evaluate ongoing

and future hydroclimate change in the arid western Chinese Loess Plateau (WCLP), a

region with increasing demand for water resources due to the increasing population

and socioeconomic activities. Here we present a new tree-ring chronology inform the

WCLP, which shows coherent interannual variations with tree-ring chronologies from

7 neighboring areas across the WCLP, suggesting a common regional climate control

over tree growth. However, considerable differences are observed among their

interdecadal variations, which are likely due to growth disturbances at interdecadal

timescales. To deal with this issue, we use a frequency based method to develop a

composite tree-ring chronology from 401 tree-ring series from these 8 sites, which

shows more pronounced interdecadal variability than a chronology developed using

traditional methods. The composite tree-ring chronology is used to reconstruct the

annual precipitation from previous August to current July from 1568 to 2012,

extending about 50 years longer than the previous longest tree-ring reconstruction

from the region. The driest epoch of our reconstruction is found in the 1920s-30s,

which matches well with droughts recorded in historical documents. Over the past

four centuries, a strong resemblance between drought variability in the WCLP and

western North America (WNA) is evident on multidecadal timescales, but this

relationship breaks down on timescales shorter than about 50 years.

44

1 Introduction

Hydroclimate in the western Chinese Loess Plateau (WCLP), a boundary region of the Asian summer monsoon, is sensitive to large-scale climate anomalies (Chen et al., 2014). In this arid to semi-arid region, water availability is the major limiting factor for ecological protection, agricultural and industrial activities. Thus, improved understanding of hydroclimate regimes in the WCLP will not only add new knowledge to climate science, but also provide means to better plan future development in a sustainable way (Ren and Walker, 1998). However, the lack of instrumental data in the WCLP before the 1950s limits our ability to place recent hydroclimate conditions in a long term context. As a result, hydroclimate variations at long timescales, e.g. multi-decadal, are difficult to examine using instrumental data.

The shortness of the instrumental records can be alleviated by employing climate proxies such as tree rings to extend the observations back in time (Fritts, 1976). Although many tree-ring based reconstructions have been developed with the aim to understand hydroclimate changes in the WCLP and surroundings (Fang et al., 2010; Gou et al., 2015; Hughes et al., 1994; Kang et al., 2012; Li et al., 2007; Liang et al., 2006; Liu et al., 2008; Shao and Wu, 1994; Yang et al., 2012), the lengths of the reconstructions seldom exceed 400 years, and the spatial coverage can be improved.

67　In this study, we collected new tree-ring samples in Weiyuan county of the Gansu

68　province in the WCLP to improve the temporal and spatial coverage of tree-ring data

69　in the region. Also, by combining both new and previously published data we

70　generated an improved and extended annual precipitation reconstruction for the entire

71　WCLP. For the reconstruction to express regionally coherent variability, we

72　introduced a frequency-based method to generate a composite chronology, which was

73　expected to have better performance in retaining interdecadal climate information

74　than when traditional methods are used. Finally, we investigated linkages between

75　hydroclimate reconstructions in the WCLP and climate sensitive tree-ring

76　chronologies from eastern Asia and North America to put the new reconstruction into

77　the perspective of large-scale hydroclimate teleconnections.

78

79　**2 Data and methods**

80　2.1 Tree-ring data

81　The southwestern part of the WCLP is a transitional area from the Chinese Loess

82　Plateau to world's highest plateau, the Tibetan Plateau (Figure 1), and tree-ring

83　samples were collected in the Dieshan and Songmingyan Mountains (Fang et al.,

84　2015). The southeastern part of the WCLP also includes the western part of the

85　Qinling Mountain, a geographic boundary separating southern and northern China.

86　Precipitation associated with the Asian summer monsoon allows a dominance of

87　broadleaf forests (Figure 1). Conifers are often found on mountain peaks or cliff areas

88　with very shallow soils (Fang et al., 2015). Precipitation decreases sharply from the

89 southwestern and southeastern parts to the core regions of the WCLP which is

90 dominated by loess sediments and the Gobi desert. Old growth forests in the study

91 region are mainly found in mountains with exposed bedrock, but rarely on the

92 commonly distributed loess mountains, likely because the bedrock provides a higher

93 ability to retain moisture than the porous loess sediments (Fang et al., 2012). These

94 mountains are known as "green islands" in this region, and tree-ring material has

95 previously been collected from the Helan, Xinglong, Guiqing and Kongtong

96 Mountains (Fang et al., 2015; Li et al., 2007), as well as the Shouyang Mountain and

97 the Diaoling Temple sites presented in this study (Figure 1).

98

99 The Shouyang Mountain (35.03 ^{o}N, 104.32 ^{o}E) and Diaoling Temple (35.1^{o}N,

100 104.17^{o}E) sites are located near the Lianfeng and Qingyuan village of the Weiyuan

101 county, respectively. Both sites only have a few old-growth trees surrounding the

102 temples which were sampled. We took 9 increment cores from 4 old *Pinus*

103 *tabulaeformis* trees at Shouyang Mountain and 22 cores from 11 old *Pinus*

104 *tabulaeformis* trees at Diaoling Temple site. It should be noted that trees near temples

105 are likely influenced by human activities. For example, it is known that local people

106 ocassionally collected snow from the surroundings to place under the trees in winter

107 and watered trees in summer to avoid drought stress. Unfortunately, old growth trees

108 suitable for climate reconstruction in this area can mostly be found near the temples,

109 since they are protected from logging due to the religious purposes. Even so, these

110 tree-ring series are still found to be quite sensitive to climate as indicated by the

111   significant climate-growth correlations shown below. These samples were mounted,

112   air dried and polished following standard dendrochronological methods (Stokes and

113   Smiley, 1968), and then crossdated by checking the matching patterns of extremely

114   narrow and wide rings. The crossdated samples were measured and the quality of the

115   crossdating was checked using the program COFECHA (Holmes, 1983). In addition,

116   we found that the crossdated tree-ring width series from Shouyang Mountain and

117   Diaoling Temple were significantly correlated with previously published tree-ring

118   series from neighboring sites (Fang et al., 2015; Li et al., 2007). Overall, 401 of the

119   total 603 tree-ring series from the region could be crossdated. The moderate ratio of

120   selected vs. available tree-ring series being useful for the chronology development

121   was largely because of the large distances among these sites. Also, to maintain the

122   robustness of the composite chronology, only the tree-ring series that were highly

123   correlated (r>0.5, p<0.001) were selected. This strict selection criterion excluded

124   many tree-ring series. The selected tree-ring series included 15 out of the 31 cores

125   from our sampling sites, 42 out of the 107 cores from Helan Mountain, 123 out of the

126   200 cores from Xinglong Mountain, 30 out of the 43 cores from Guiqing Mountain,

127   30 out of the 70 cores from Xiaolong Mountain, 45 out of the 52 cores from

128   Kongtong Mountain, 99 out of the 101 cores from Dieshan Mountain and 17 out of

129   the 30 cores from Songmingyan Mountain (Figure 1). Chronologies of individual sites

130   developed from selected tree-ring series match with each other better than the

131   chronologies developed from all series as indicated by the relatively higher

132   correlations among the chronologies of individual sites using selected series (Figure

S1). In addition, we identified a missing ring in 1770 for all tree-ring cores from the Guiqing and Xiaolong Mountains. This missing ring had not been identified previously because of insufficient number of long tree-ring series extending beyond 1770 at these sites.

2.3 Methods

The 8 individual site tree-ring chronologies were developed using a traditional method, and composite WCLP tree-ring chronologies, based on the selected series from all the sites, were developed using two different methods: a traditional and a new frequency-based method. In the traditional method, all tree-ring series at the individual sites were fitted by a smoothed cubic spline curve with a 50% frequency cutoff of 180 years, which is equal to the mean length of the all the series, to remove the age-related growth trends. The detrended tree-ring indices were averaged following a biweight robust mean methodology to produce a chronology (Cook, 1985). The reliable portion of the tree-ring chronologies was determined when the statistic of the subsample signal strength (SSS) is higher than 0.85 (Wigley et al., 1984). The composite chronology based on the traditional method is henceforth referred to as standard.

The frequency-based method for the composite chronology development was designed to better retain interdecadal climate information by dampening the site-specific, non-climatic influences on these interdecadal timescales. We employed a

155   10 point butterworth filter (Ghil et al., 2002; Mann et al., 2009) to decompose the

156   tree-ring indices into interannual ($f>0.1$) and interdecadal ($f<0.1$) variations. This

157   filter has advantages in simulating the passband due to its quite flat frequency

158   response in the passband (Ghil et al., 2002; Mann et al., 2009). The interannual

159   variations generally matched well, which were thus averaged to highlight the common

160   interannual variations of the chronology using the biweight robust mean method

161   (Cook, 1985). We found that some interdecadal variations of tree-ring series were

162   common across the sites while others differed (detailed below). These differing

163   interdecadal variations are likely caused by non-climatic factors (Björklund et al.,

164   2013). To enhance the common interdecadal climate signal, the composite chronology

165   was developed by using only those chronologies with well-matched interdecadal

166   variations. Herein, to define the tree rings with coherent variations, we selected those

167   having high loadings (>0.5) on the first principal component, representing their

168   common interdecadal variations, based on all the data.

169

170   In order to take advantage of the long tree-ring series, we employed a nested approach

171   (Cook et al., 2002) by iteratively stepwise identifying the series with common

172   interdecadal variations from the most replicated common period to the longest period

173   at a step of 25 years. All of the nested chronologies were standardized to have equal

174   mean and variance in the most replicated common period and then averaged. The final

175   composite chronology was developed by merging the interannual and interdecadal

176   chronologies. This frequency based method was designed to deal with the site-specific,

8

177   non-climatic variations at interdecadal timescale, and differs from the previous

178   Hilbert-Huang Transform (HHT) based method that aims to remove the tree-specific

179   non-climatic variations of tree growths at a site (Fang et al., 2013).

180

181   Monthly temperature and precipitation data were obtained from the meteorological

182   stations at Lintao, Minxian, Lanzhou, Tianshui, Pingliang and Yinchuan, which are

183   located close to the tree-ring sites (see Figure 1). The instrumental data started in

184   1951 when most of the stations were established. The monthly climate data from these

185   stations were averaged and the climate-growth relationships were analyzed from the

186   start of the previous growing season (May) to the end of the current growing season in

187   October (Fang et al., 2015). To identify the strongest climate-growth relationships, we

188   calculated the correlations between tree growth and all possible combinations of

189   monthly total precipitation and mean temperature, which resulted in 444 climate

190   variables. The robustness of the reconstruction was tested using a split calibration and

191   verification procedure (Meko and Graybill, 1995) by calibrating the tree rings using

192   instrumental data from 1951-1981 and from 1982-2012, which were verified using the

193   rest of data from 1982-2012 and 1951-1981, respectively. The statistics of sign test

194   (ST), reduction of error (RE) and coefficient of efficiency (CE) were used to examine

195   the robustness of the reconstruction, where RE and CE values greater than zero

196   indicate acceptable reconstruction ability (Cook et al., 2010). To further validate the

197   reconstruction, we used a set of drought reconstructions based on historical

198   documents (Zhang et al., 2003) from 12 counties surrounding the tree-ring sites in the

199 WCLP, including Shanba, Etuoke, Zhangye, Yulin, Yinchuan, Xining, Yan'an,

200 Lanzhou, Pingliang, Tianshui, Xi'an, Hanzhong (Figure 1) as independent data. This

201 historical drought atlas classified drought into five categories from 1 to 5 to

202 representing extremely wet, moderately wet, normal, moderately dry and extremely

203 dry conditions, respectively. The documents based drought reconstructions start in

204 1470 and contain some missing values in the early periods due to insufficient

205 historical records. We calculated the mean of these drought reconstructions from

206 historical documents to represent the regional drought variations.

207

208 **3 Results**

209 3.1 A composite WCLP tree-ring chronology

210 The interannual and interdecadal variations of the 8 tree-ring width chronologies in

211 the study are shown in Figure 2. The interannual variations are highly correlated

212 among the sites (Figure 2a). However, there are conspicuous mismatches of

213 interdecadal variations among these chronologies, particularly in the 1820s-1850s and

214 the 1850s-1870s (Figure 2b). Both the mean correlations (r=0.72) and effective

215 freedom (126.7) based on the Chelton methods (Pyper and Peterman, 1998) are higher

216 for the correlations among the interannual variations than those for the interdecadal

217 variations (r=0.63, effective freedom=33.2). High correlations on the interannual

218 timescale indicate a common forcing on tree growth in the region. The differences in

219 interdecadal growth variability among the sites, however, are likely caused by

220 site-specific non-climatic factors and consequently need to be minimized when

221 developing a regional composite chronology. Similar features have been found for the

222 paired correlations among individual tree-ring chronologies of the 8 areas with more

223 significant correlation among the high-passed (f>0.1) chronologies than the

224 low-passed data (Table S2). Although there are paired chronologies with moderate

225 correlations, the composite chronology were developed based only on those highly

226 correlated tree-ring series as indicated above. It is unlikely that climate regimes differ

227 among these neighboring sites on interdecadal timescales for this area with its

228 coherent interannual climate patterns, because the interdecadal climate regimes often

229 varies over large spatial areas. Moreover, at each site the tree-ring series displayed

230 common interdecadal variations, further supporting that mismatches among

231 interdecadal variations are not related to climate.

232

233 We generated one high-frequency mean chronology based on all the 401 tree-ring

234 width data with coherent variations (Figure 3a) and one low-frequency mean

235 chronology from 131 tree-ring series displaying coherent interdecadal variations

236 (Figure 3b). The frequency based composite chronology has enhanced interdecadal

237 variability (Figure 3c). The enhancement on the interdecadal variability is not very

238 pronounced likely related to the close interannual variability that "blurred" the

239 interdecadal variability. As shown in Figure 4, the frequency based chronology

240 developed from the selected tree-ring series with coherent interdecadal variations

241 showed stronger interdecadal variability than the standard chronology based on all the

242 tree-ring series including some series with divergent interdecadal variations.

243

The interdecadal variations of the tree-ring chronology agree well with those from the

drought reconstruction based on historical documents (Figure 4). Good matches

between moisture sensitive tree rings and historical documents in this area have been

revealed in previous studies (Liang et al., 2006; Yang et al., 2014a; Yang et al., 2014b),

validating our use of tree rings for hydroclimate reconstruction in the following

section. Mismatches between the two types of records are mainly observed before

1640, which may be due to the relatively few historical documents and low number of

the tree-ring series included in the frequency based composite chronology in these

early periods. Previous comparisons between tree rings and historical documents also

indicated mismatches in these early periods (Yang et al., 2014a). The reliable portion

of the composite chronology, based on an EPS value greater than 0.85 is from 1568 to

2012 (Figure 3c), which is about 50 years longer than the previously published

longest chronology from the WCLP region (Fang et al., 2012).

257

258 3.2 Precipitation reconstruction of WCLP

The composite WCLP chronology show positive correlations with precipitation and

negative correlations with temperature in previous and current growing seasons

(Figure 5). Tree growth shows highest correlations with precipitation of a

hydrological year starting in August prior to growth and ending in July of the growth

year (r=0.66) (Figure 5), thus integrating precipitation signals over two years. Similar

responses to hydroclimate (or precipitation) have also been found in trees growing in

265   arid regions near the Tibetan Plateau (Fang et al., 2015).

266

267   The previous August to current July WCLP precipitation reconstruction, based on the

268   composite chronology, explains 43.1% of the instrumental variance (Figure 6). The

269   correspondence between the reconstructed and observed precipitation is given in

270   Figure 6a. The ST for both tests are significant (p<0.01), and the RE and CE for both

271   tests are 0.45 and 0.36 respectively, indicating acceptable reconstruction skill. We

272   identified extreme dry (<2SD) years in 1770, 1796, 1831, 1928, 1929 and 1932

273   (Figure 6b), and extremely dry epochs, defined as at least 5 persistently dry (<1SD)

274   years from the low-passed (f<0.1) data, during 1702-1707, 1716-1724, 1734-1737,

275   1827-1833, 1862-1866, and 1925-1933. The dry epoch from 1925-1933 was the most

276   severe during the last four centuries, with 3 extremely dry years falling within this

277   period. Extremely wet years (>2SD) were found in 1603-1607, 1751, 1753, 1755,

278   1786, 1803-1805, 1807, 1977, 1979 and 1980. Wet epochs were found in 1601-1610,

279   1750-1756, 1783-1792, 1801-1808, 1853-1857, 1963-1967 and 1976-1981. Many of

280   the reconstructed extreme dry/wet years or periods have previously been revealed by

281   independent tree-ring data in the WCLP and its surroundings (Gou et al., 2015; Kang

282   et al., 2014; Kang et al., 2012; Liang et al., 2006; Yang et al., 2012). Our

283   reconstruction also shows similar variations as the mean of the gridded reconstruction

284   in the study region (averaged over 102 ^{o}E-108 ^{o}E; 35 ^{o}E-40 ^{o}E) from the Monsoonal

285   Asia Drought Atlas (Cook et al., 2010) (Figure S2). However, our reconstruction

286   shows stronger interdecadal variability than the one from the Monsoonal Asia

287   Drought Atlas, which is consistent with above results of the enhanced interdecadal

288   variability of the tree-ring chronology using the new method.

289

290   **4 Discussion**

291   4.1 Influences of non-climatic factors on interdecadal variations of tree rings

292   It is generally believed that the influences of non-climatic factors on individual

293   tree-ring series can be cancelled out when developing a tree-ring chronology by

294   averaging numerous tree-ring series at a site, assuming that the common variation in

295   tree growth is climate related (Fritts, 1976). Our study highlights that interdecadal

296   variations caused by non-climatic factors are less likely to be averaged out during the

297   chronology development process than interannual variations. This may largely be

298   because non-climatic disturbances often affect similar number of biases at growth at

299   interdecadal and interannual scales while the number of interdecadal variations is

300   much lower than the interannual variations, causing higher ratio of biases at

301   interannual scale than at interannual scale. An example of a non-climate related

302   disturbances is a growth release episode of 20 years which is observed in a tree-ring

303   series of 100 years: it can cause the ratio of biased growth of 1% at the interannual

304   timescale but can cause the ratio of biased growth of 20% at the interdecadal

305   timescale.

306

307   Non-climatic factors causing different interdecadal variations among sites can be

308   human-related activities and/or natural processes. For example, enhanced tourism

309   activities at many sites in the WCLP may have caused growth suppressions of some

310   old trees near the temples. Logging activities can cause growth release of neighboring

311   trees (Björklund et al., 2013; Latham and Tappeiner, 2002; Martín-Benito et al., 2010).

312   The natural ecological processes causing different interdecadal tree-ring variations

313   can be related to growth suppression or release due to completion from neighboring

314   trees. The commonly used crossdating method ensures the match of high-frequency

315   variations of tree rings, but cannot guarantee matches of the interdecadal variations.

316   Accordingly, our frequency based method identified the sites with similar climate

317   patterns, as indicated by coherent interannual variations, and then only the tree-ring

318   series with coherent interdecaldal variations across sites were used to develop the

319   final composite chronology.

320

321   It is common in dendroclimatology to compare regional tree-ring based climate

322   reconstructions with reconstructions in surrounding regions to explore any climatic

323   linkages. However, such comparisons often find temporally varying associations on

324   interdecadal timescales. Our study suggests that such mismatches at interdecadal

325   timescale could partly be caused by different non-climatic factors. The frequency

326   based method can enhance the climate signal for a large region at interdecadal

327   timescale, facilitating investigations of climate linkages across regions. As shown in

328   Figure S3, the frequency-based chronology has good ability in retaining the regional

329   climate signals at interdecadal scale. Still, it should be kept in mind that local climate

330   signals might be dampened by merging tree-ring data across sites, if there is a low

331   number of tree-ring series with coherent interdecadal variations with the regional

332   chronology. For example, the local climate signals of the Helan Mountain area were

333   not well retained because only a few tree-ring series from that region were included in

334   the regional chronology. To test whether local climate signals are removed or not,

335   independent proxy data, such as historical documents, should be used.

336

337   4.2 Droughts in the WCLP

338   Instrumental records and paleoclimate reconstructions have previously revealed

339   similar precipitation regimes between the WCLP and northeastern Asia (Fang et al.,

340   2012; Li et al., 2009; Pederson et al., 2001). Such co-variability is reasonable, as these

341   regions are situated in the marginal areas of Asian summer monsoon. For example,

342   the timing of the two most severe reconstructed droughts in our study region in the

343   1920s-1930s and the 1720s-1730s agrees with droughts in northeastern China and

344   eastern Mongolia (Fang et al., 2010; Li et al., 2009; Liang et al., 2006; Pederson et al.,

345   2001). Some dry events were likely caused by weakening of the Asian summer

346   monsoon. For example, one of the driest years in the WCLP was found in 1796, which

347   corresponds to a severe El Niño year (Grove, 2007). El Niño episodes are associated

348   with colder-than-normal western equatorial Pacific Ocean, and thus reduced

349   convective activities, which can weaken the Asian summer monsoon and thus cause

350   dry condition in its front regions (Ju and Slingo, 1995).

351

352   Although drought variations in the WCLP have consistencies with those in other

353 marginal monsoon areas, the degrees of dryness in these marginal areas can be

354 different. Based on our drought reconstruction for the entire WCLP, the driest period

355 during the past four centuries was in 1925-1933. This drought, which has been widely

356 described in historical documents, was observed in over 20 provinces in China (Li,

357 1994; Liang et al., 2006), as well as inferred from stalagmite records in the WCLP

358 (Zhang et al., 2008) and tree-ring data from northeastern and central Mongolia

359 (Pederson et al., 2001). Between 1928 and 1933, the drought induced serious

360 reduction in food productivity causing a famine that killed about 2.5 to 3 million

361 people, which was about half of the population in the Gansu province covering most

362 of our study region (Li, 1994).

363

364 Other studies have suggested that the drought in the 1630s-1640s, which may have

365 contributed to the fall of the Chinese Ming Dynasty, was the severest during the past

366 four centuries in the marginal areas of the Asian summer monsoon (Cook et al., 2010;

367 Zhang et al., 2008). However, according to our reconstruction, this period was only

368 moderately dry in the WCLP (Figure 6). This is likely because the 1920s-1930s

369 drought was centered over the WCLP, while the 1630s-1640s drought was centered

370 over northeastern China (Cook et al., 2010; Li, 1994; Zhang et al., 2008). Another dry

371 period that had its core area in northeastern China, but still affecting the WCLP, was

372 the "Great Victorian Drought" from 1876-1878, which has been recorded in both

373 tree-ring data (Cook et al., 2010) and historical documents (Li, 1994). Regional

374 differences among these extended droughts suggest that the dynamics of the Asian

375 summer monsoon is spatially variable in its boundary regions, with droughts of

376 different magnitude centered in different sub-regions.

377

378 4.3 Co-varying climate changes in the WCLP and western North America (WNA)

379 Compared to other paleoclimate proxies, tree-ring data have advantages to facilitate

380 investigations of large-scale climate changes due to their large and dense spatial

381 coverage (Fritts, 1976). To explore the linkages with large-scale climate patterns, we

382 compared our WCLP reconstruction with other climate sensitive tree-ring

383 chronologies (Table S1) from Eastern Asia and North America (Figure 7), as

384 hydroclimate changes in this pan-Pacific area haven been revealed to be closely

385 linked (Fang et al., 2016). The tree-ring chronologies were mainly derived from the

386 drought Atlas in Asia and North America (Cook et al., 2010; Cook et al., 2004) and

387 the PAGES 2k dataset (PAGES 2k Consortium, 2013). Our composite chronology

388 shows significant correlations at multi-decadal scales with other tree-ring

389 chronologies in distant regions, particularly in WNA(Figure 7a and 7b). On the

390 interannual timescales, high correlations are only obtained with tree-ring chronologies

391 in neighboring regions (Figure 7c and 7d). There may be different controlling factors

392 for regional precipitation at different timescales. Locally consistent variations in tree

393 rings in the neighboring areas may suggest the dominance of local surface conditions,

394 such as vegetation cover and topographic features, which can modulate the local

395 water cycles through, for example, the soil moisture content, evaporation, convection

396 and nuclei formations (Huang et al., 2015). On the other hand, co-variability of

397   multi-decadal precipitation variability across remote regions indicates that large-scale

398   circulation pattern play a larger role at these timescale. This is because large-scale

399   oceanic and atmospheric patterns are more likely to cause concurrent climate

400   anomalies in distant regions through teleconnections compared to local water cycles

401   (Li et al., 2013; Ortega et al., 2015). In addition, the WCLP-WNA hydroclimate

402   linkages are likely part of the large-scale climate linkages between eastern Asia and

403   North America (Figure S4). The WCLP and WNA appear to among the key regions

404   showing close linkages between climate changes in eastern Asia and North America

405   over the past 4 centuries (Figure S4).

406

407   This study highlights the timescale dependency of climate regimes, which can vary

408   when certain threshold timescale is crossed. For example, climate change between our

409   study region and WNA has almost no linkage (Figure 8a) on interannual timescale,

410   but they have close matches at multi-decadal timescales (Figure 8b). The

411   WCLP-WNA co-variability sharply becomes significant at a threshold timescale of ~

412   50 years, suggesting that the controlling climate factors on this co-variability have

413   periodicities over ~50 years. We thus investigate the possible causes of the linkages

414   between our reconstruction and climate in WNA at multi-decadal timescale only.

415

416   To further test whether our reconstruction reveals large-scale climate patterns, we

417   compared our reconstruction with reconstructions of large-scale climate patterns. At

418   multi-decadal timescale, the Pacific climate is largely modulated by the Pacific

419 Decadal Oscillation (PDO) (Mantua and Hare, 2002), which is considered as the

420 norther part of the Interdecadal Pacific Oscillation (IPO) (Henley et al., 2015).

421 However, the existing PDO reconstructions have considerable mismatches among

422 each other, which provided different depending on PDO reconstructions used

423 (Kipfmueller et al., 2012). We thus employed an IPO reconstruction based on

424 tree-ring data of the Pacific area that revealed coherent interdecadal climate patterns

425 over the entire Pacific Ocean area (Fang et al., 2016). The IPO is also documented to

426 have a strong impact on global climate at multi-decadal/interdecadal timescale (Dai et

427 al., 2015; Kosaka and Xie, 2013). Apart from IPO, the Atlantic Multi-decadal

428 Oscillation (AMO) has been widely recognized to have strong modulation on

429 multi-decadal climate variability across the globe (Schlesinger and Ramankutty, 1994;

430 Sonechkin et al., 1999). Proxies from both the Atlantic and Pacific regions have

431 revealed AMO signals (Gray et al., 2004; Wang et al., 2011). The AMO

432 reconstructions are robust at multi-decadal timescale since the reconstructions using

433 proxies from independent sources in Atlantic and Pacific regions have similar

434 multi-decadal variability. We thus employed an AMO reconstruction by Gray et al.

435 (2004) based on proxies from Atlantic regions. As shown in Figure 8c, our

436 reconstruction agrees well with the IPO reconstruction, where almost all cycles match.

437 This suggests that the multi-decadal variability of the WCLP is modulated by the IPO

438 and our study region is one of the key regions linked to IPO variability. However,

439 how IPO modulates regional climate, and thus tree-ring growths, is still uncertain

440 because the shortness of the instrumental data for this region. Our results suggest that

441 there is a possibility that the IPO modulates multi-decadal temperature and/or

442 precipitation to cause regional multi-decadal climate change.

443

444 **5 Conclusions**

445 Our newly developed tree-ring series at Shouyang Mountain and Diaoling Temple

446 sites are highly correlated at interannual timescale with most of the moisture sensitive

447 tree-ring series from 7 surrounding areas in the WCLP, suggesting a common

448 precipitation regime in the region. However, mismatches were observed of the

449 interdecadal variations among the tree-ring data in the region, which are likely caused

450 by local non-climatic disturbances. This study highlights that non-climatic

451 disturbances at interdecadal timescale are less likely to be averaged out during the

452 chronology development process relative to disturbances at interannual timescale. To

453 enhance the common climate signal also on interdecadal timescales, we used a

454 frequency based method to develop the regional composite chronology which only

455 included tree-ring series with coherent interdecadal variations across sites.

456

457 We used 401 tree-ring series to develop a composite chronology for the WCLP

458 spanning from 1568 to 2012, which is about 50 years longer than the previously

459 published one. The frequency based tree-ring chronology showed stronger

460 interdecadal variations than the chronology built using traditional methods. It was

461 used to reconstruct the annual precipitation from previous August to current July back

462 to 1568, whiere the reconstruction explained 43.1% of the instrumental variance.

463 Interdecadal drought variations revealed in this tree-ring based reconstruction agree

464 well with the drought histories recorded in historical documents. Reconstructed

465 precipitation variability in the WCLP was very similar to the drought variability in the

466 WNA at multi-decadal (f<0.02) timescales, while no linkage was found in the higher

467 frequencies. This linkage at multi-decadal timescales is likely due to the common

468 influences of the IPO on hydroclimate in the two regions.

469

470

471

472

473

474

475

476

477

478

485

486

487

488

489

490

491

492

493

494

495

496

497

498

499

500

References

Björklund JA, Gunnarson BE, Krusic PJ, Grudd H, Josefsson T, Östlund L, Linderholm HW (2013) Advances towards improved low-frequency tree-ring reconstructions, using an updated Pinus sylvestris L. MXD network from the Scandinavian Mountains. Theoretical and applied climatology 113: 697-710

Chen J, Chen F, Feng S, Huang W, Liu J, Zhou A (2014) Hydroclimatic changes in

23

507   China and surroundings during the Medieval Climate Anomaly and Little Ice

508   Age: Spatial patterns and possible mechanisms. Quaternary Science Reviews 107:

509   98–111

510 Cook E, Anchukaitis KJ, Buckley BM, D'Arrigo RD, Jacoby GC, Wright WE (2010)

511   Asian Monsoon Failure and Megadrought During the Last Millennium. Science

512   328: 486-489

513 Cook E, Seager R, Cane MA, Stahle DW (2007) North American drought:

514   reconstructions, causes, and consequences. Earth-Sci Rev 81: 93-134

515 Cook E, Woodhouse CA, Eakin CM, Meko DM, Stahle DW (2004) Long-term aridity

516   changes in the western United States. Science 306: 1015

517 Cook ER (1985) A time series analysis approach to tree ring standardization. vol PhD.

518   The University of Arizona, Tucson, USA

519 Cook ER, D'Arrigo RD, Mann ME (2002) A well-verified, multiproxy reconstruction

520   of the winter North Atlantic Oscillation Index since ad 1400. Journal of Climate

521   15: 1754-1764

522 Dai A, Fyfe JC, Xie SP, Dai X (2015) Decadal Modulation of Global Surface

523   Temperature By Internal Climate Variability. Nature Climate Change 5: DOI:

524   10.1038/NCLIMATE2605

525 Fang K, Cook E, Guo Z, Chen D, Ou T, Frank D, Zhao Y (2016) Synchronous

526   multi-decadal tree-ring patterns of the Pacific areas reveal dynamics of the

527   Interdecadal Pacific Oscillation (IPO) since 1567 In review

528 Fang K, Frank D, Gou X, Chen F, Liu C, Li J, Li Y (2013) Precipitation variations

529   over the past four centuries in the Dieshan Mountain area inferred from tree rings:

530   an introduction to a HHT-based method. Global and Planetary Change doi:

531   10.1016/j.gloplacha.2013.04.010

532   Fang K, Frank D, Zhao Y, Zhou F, Seppä H (2015) Moisture stress of a hydrological

533   year on tree growth in the Tibetan Plateau and surroundings. Environmental

534   Research   Letters   10:   034010,

535   doi:034010.031088/031748-039326/034010/034013/034010

536   Fang K, Gou X, Chen F, D'Arrigo R, Li J (2010) Tree-ring based drought

537   reconstruction for the Guiqing Mountain (China): linkages to the Indian and

538   Pacific Oceans. Int J Climatol 30: 1137-1145

539   Fang K, Gou X, Chen F, Liu C, Davi N, Li J, Zhao Z, Li Y (2012) Tree-ring based

540   reconstruction of drought variability (1615–2009) in the Kongtong Mountain

541   area, northern China. Global and Planetary Change 80-81: 190-197

542   Fritts HC (1976) Tree rings and climate. Academic Press, New York

543   Ghil M, Allen M, Dettinger M, Ide K, Kondrashov D, Mann M, Robertson AW,

544   Saunders A, Tian Y, Varadi F (2002) Advanced spectral methods for climatic

545   time series. Reviews of geophysics 40: 3-1-3-41

546   Gou X, Deng Y, Gao L, Chen F, Cook E, Yang M, Zhang F (2015) Millennium

547   tree-ring reconstruction of drought variability in the eastern Qilian Mountains,

548   northwest China. Climate Dynamics 45: 1761-1770

549   Gray ST, Graumlich LJ, Betancourt JL, Pederson GT (2004) A tree-ring based

550   reconstruction of the Atlantic Multidecadal Oscillation since 1567 AD.

551   Geophysical Research Letters 31: L12205. DOI: 12210.11029/12004GL019932

552 Grove RH (2007) The Great El Niño of 1789–93 and its Global Consequences

553   Reconstructing an Extreme Climate Event in World Environmental History. The

554   Medieval History Journal 10: 75-98

555 Henley BJ, Gergis J, Karoly DJ, Power S, Kennedy J, Folland CK (2015) A tripole

556   index for the interdecadal Pacific oscillation. Climate Dynamics 45: 3077-3090

557 Hoerling M, Kumar A (2003) The perfect ocean for drought. Science 299: 691-694

558 Holmes RL (1983) Computer-assisted quality control in tree-ring dating and

559   measurement. Tree-ring bull 43: 69-78

560 Huang J, Yu H, Guan X, Wang G, Guo R (2015) Accelerated dryland expansion under

561   climate change. Nature Climate Change

562 Hughes MK, Wu X, Shao X, Garfin GM (1994) A Preliminary Reconstruction of

563   Rainfall in North-Central China since A.D. 1600 from Tree-Ring Density and

564   Width. Quaternary Research 42: 88-99

565 Ju J, Slingo J (1995) The Asian summer monsoon and ENSO. Quarterly Journal of the

566   Royal Meteorological Society 121: 1133-1168

567 Kang S, Bräuning A, Ge H (2014) Tree-ring based evidence of the multi-decadal

568   climatic oscillation during the past 200 years in north-central China. Journal of

569   Arid Environments 110: 53-59

570 Kang S, Yang B, Qin C (2012) Recent tree-growth reduction in north central China as

571   a combined result of a weakened monsoon and atmospheric oscillations.

572   Climatic Change 115: 519-536

573   Kipfmueller KF, Larson ER, St George S (2012) Does proxy uncertainty affect the

574   relations inferred between the Pacific Decadal Oscillation and wildfire activity in

575   the western United States? Geophysical Research Letters 39: DOI:

576   10.1029/2011GL050645

577   Kosaka Y, Xie S-P (2013) Recent global-warming hiatus tied to equatorial Pacific

578   surface cooling. Nature 501: 403-407

579   Latham P, Tappeiner J (2002) Response of old-growth conifers to reduction in stand

580   density in western Oregon forests. Tree Physiology 22: 137-146

581   Li J, Chen F, Cook ER, Gou X, Zhang Y (2007) Drought reconstruction for north

582   central China from tree rings: the value of the Palmer drought severity index. Int

583   J Climatol 27: 903-909

584   Li J, Cook ER, Chen F, Davi N, D'Arrigo R, Gou X, Wright WE, Fang K, Jin L, Shi J

585   (2009) Summer monsoon moisture variability over China and Mongolia during

586   the past four centuries. Geophysical Research Letters 36: L22705

587   doi:22710.21029/22009GL041162

588   Li J, Xie SP, Cook E, Morales MS, Christie DA, Johnson NC, Chen F, D'Arrigo R,

589   Fowler AM, Gou X, Fang K (2013) El Niño Modulations over the Past Seven

590   Centuries: Amplitude, Teleconnection, and the Volcanic Effect. Nature Climate

591   Change 3: DOI: 10.1038/NCLIMATE1936

592   Li W (1994) The top ten famine in recent China. Shanghai People's Press

593   Liang E, Liu X, Yuan Y, Qin N, Fang X, Huang L, Zhu H, Wang L, Shao X (2006)

594   The 1920s drought recorded by tree rings and historical documents in the

595   semi-arid and arid areas of northern China. Climatic Change 79: 403-432

596   Liu Y, Cai Q, Liu W, Yang Y, Sun J, Song H, Li X (2008) Monsoon precipitation

597   variation recorded by tree-ring δ 18 O in arid Northwest China since AD 1878.

598   Chemical Geology 252: 56-61

599   MacDonald GM, Case RA (2005) Variations in the Pacific Decadal Oscillation over

600   the   past   millennium.   Geophys   Res   Lett   32:   L08703,

601   doi:08710.01029/02005GL022478

602   Mann ME, Zhang Z, Rutherford S, Bradley RS, Hughes MK, Shindell D, Ammann C,

603   Faluvegi G, Ni F (2009) Global signatures and dynamical origins of the Little Ice

604   Age and Medieval Climate Anomaly. Science 326: 1256-1260

605   Mantua NJ, Hare SR (2002) The Pacific decadal oscillation. Journal of Oceanography

606   58: 35-44

607   Martín-Benito D, Del Río M, Heinrich I, Helle G, Cañellas I (2010) Response of

608   climate-growth relationships and water use efficiency to thinning in a Pinus nigra

609   afforestation. Forest Ecology and Management 259: 967-975

610   Meko D, Graybill DA (1995) Tree-ring reconstruction of upper Gila river discharge. J

611   Am Water Resour As 31: 605-616

612   Ortega P, Lehner F, Swingedouw D, Masson-Delmotte V, Raible CC, Casado M, Yiou

613   P (2015) A model-tested North Atlantic Oscillation reconstruction for the past

614   millennium. Nature 523: 71-74

615   PAGES 2k Consortium (2013) Continental-scale temperature variability during the

616   past two millennia. Nature Geoscience 6   339-346

617 Pederson N, Jacoby GC, D'Arrigo RD, Cook ER, Buckley BM, Dugarjav C, Mijiddorj

618   R (2001) Hydrometeorological Reconstructions for Northeastern Mongolia

619   Derived from Tree Rings: 1651-1995. J Climate 14: 872-881

620 Pyper BJ, Peterman RM (1998) Comparison of methods to account for autocorrelation

621   in correlation analyses of fish data. Canadian Journal of Fisheries and Aquatic

622   Sciences 55: 2127-2140

623 Ren M-e, Walker JH (1998) Environmental consequences of human activity on the

624   Yellow River and its delta, China. Physical Geography 19: 421-432

625 Ruddiman W (2014) Earth's Climate: past and future. W H Freeman & Company,

626   New York

627 Schlesinger ME, Ramankutty N (1994) An oscillation in the global climate system of

628   period 65-70 years. Nature 367: 723-726

629 Seidel DJ, Fu Q, RanDel WJ, ReichleR TSJ (2007) Widening of the tropical belt in a

630   changing climate. Nature Geoscience 1: 21-24

631 Shao X, Wu X (1994) Radial growth of Huashan Pine and its response to climate.

632   Journal of Chinese Geography 4: 88-102

633 Sonechkin D, Astafyeva N, Datsenko N, Ivachtchenko N, Jakubiak B (1999)

634   Multiscale oscillations of the global climate system as revealed by wavelet

635   transform of observational data time series. Theoretical and applied climatology

636   64: 131-142

637 Stokes MA, Smiley TL (1968) An introduction to tree-ring dating. University of

638   Chicago Press, Chicago, Illinois

639   Wang X, Brown PM, Zhang Y, Song L (2011) Imprint of the Atlantic multidecadal

640   oscillation on tree-ring widths in Northeastern Asia since 1568. PloS one 6:

641   e22740

642   Wigley TML, Briffa KR, Jones PD (1984) Average value of correlated time series,

643   with applications in dendroclimatology and hydrometeorology. J Appl Meteorol

644   Clim 23: 201-234

645   Yang B, Feng S, Sonechkin DM, Qin C (2012) Tree ring-based annual streamflow

646   reconstruction for the Heihe River in arid northwestern China from AD 575 and

647   its implications for water resource management. Holocene 22: 773-784

648   Yang B, Kang S, Ljungqvist FC, He M, Zhao Y, Qin C (2014a) Drought variability at

649   the northern fringe of the Asian summer monsoon region over the past millennia.

650   Climate dynamics 43: 845-859

651   Yang B, Qin C, Wang J, He M, Melvin TM, Osborn TJ, Briffa KR (2014b) A

652   3,500-year tree-ring record of annual precipitation on the northeastern Tibetan

653   Plateau. Proceedings of the National Academy of Sciences 111: 2903-2908

654   Zhang D, Li X, Liang Y (2003) Complementary Data of the Yearly Charts of

655   Dryness/Wetness in China for the Last 500 years Period. . Journal of Applied

656   Meteorological Science 14: 379-384

657   Zhang P, Cheng H, Edwards RL, Chen F, Wang Y, Yang X, Liu J, Tan M, Wang X

658   (2008) A test of climate, sun, and culture relationships from an 1810-year

659   Chinese cave record. Science 322: 940-942

660

661

662

663

664

665

666

667

668

669

670

671

672

673

674

675

676

677   **Figure Captions**

678   **Figure 1**. Location of the tree-ring sites developed previously and in this study, the

679   counties with historical drought archives, the meteorological stations in western

680   Chinese Loess Plateau (WCLP). The inset indicating the location of the study region

681   in eastern Asia.

682   **Figure 2**. The (a) mean running correlations between the interannual (f>0.1) and

683   interdecadal (f<0.1) variations of the tree-ring chronologies of the 8 areas based on a

684   51-year window, and the (b) visual comparisons among the interdecadal variations

685   among these chronologies in western Chinese Loess Plateau (WCLP) during their

686   common period from 1797 to 1999. The mean running correlations were determined

687   by first calculating the correlations between individual tree-ring chronologies of each

688   site and the mean of all the chronologies of 8 areas, and then the correlations for

689   individual tree-ring chronologies were averaged to produce the mean running

690   correlations.

691   **Figure 3**. The (a) mean of the interannual (f>0.1) variations of the tree-ring indices,

692   the (b) mean of the interdecadal (f<0.1) variations of the tree-ring series during their

693   common period and the (c) comparisons between the "standard chronology" and the

694   "frequency based chronology". The standard chronology was developed using

695   traditional methods by averaging all the crossdatable tree-ring indices, which have the

696   age-related growth trends being removed. The frequency based chronology was

697   produced using the introduced frequency based method, which averages the mean of

698   the interannual and the interdecadal tree-ring series, respectively. The frequency based

699   methods treats the tree-ring series at the interannual and interdecadal scale separately

700   and ensures both the interannual and interdecadal tree-ring series are well matched.

701   **Figure 4**. Comparisons among the interdecadal (f<0.1) variations of the "frequency

702   based chronology" by averaging the crossdatable tree-ring series from all sites using

703   the frequency based method, the "documents based reconstruction" of drought using

704   historical documents in western Chinese Loess Plateau (WCLP), and the "standard

705 chronology" developed calculated as the arithmetic mean of of all the tree-ring series

706 in WCLP following traditional methods.

707 **Figure 5**. Climate-growth correlations for the (a) tree-ring chronology developed for

708 the newly introduced tree rings at Shouyang Mountain and Diaolin Temple sites and

709 for the (b) composite chronology developed from tree rings at all sites. The

710 correlation coefficients with monthly temperature and precipitation were calculated

711 from the start of the previous (-) year in May till the end of the current (+) year in

712 October. The peak correlations with precipitation from previous August to current

713 July is also shown.

714 **Figure 6**. The (a) comparisons between the actual and reconstructed precipitation

715 since 1951 and the (b) drought reconstructions based on the reliable portion of the

716 tree-ring chronology since 1568.

717 **Figure 7**. Maps of (a) correlations between the low-passed (f<0.02) composite

718 tree-ring chronology in western Chinese Loess Plateau (WCLP) and the tree-ring

719 chronologies in Asia and (b) correlations between the low-passed chronology in

720 WCLP and North America (NA), (c) correlations between the high-passed (f>0.1)

721 composite chronology and the chronologies in Asia, and the (d) correlations between

722 the high-passed chronology in WCLP and chronologies in NA. The squares in maps

723 indicate the correlations between tree rings in WCLP and western NA (WNA) at the

724 multi-decadal timescale. These tree-ring chronologies derived from currently most

725 complete tree-ring datasets derived from the Monsoonal Asia Drought Atlas and the

726 North America Drought Atlas and the PAGES 2k Project. We only included the

33

727   tree-ring chronologies longer than 400 years. All the data are public avaible from

728   National Climate Data Center (NCDC).

729   **Figure 8**. The (a) comparisons between the composite tree-ring chronology in western

730   Chinese Loess Plateau (WCLP) and the mean of the tree-ring chronologies in western

731   North America (WNA), the (b) comparisons between the multi-decadal (f<0.02)

732   variations of the chronologies of WCLP and WNA and the (c) comparisons between

733   the multi-decadal variations of the chronologies of WCLP and the reconstructions of

734   the Atlantic Multi-decadal Oscillation (AMO) by Gray et al. (2004) and the

735   Interdecadal Pacific Oscillation (IPO) by Fang et al. (2016). The IPO reconstruction

736   was reversed (multiplying -1) to facilitating comparisons.

737

738

739

740

741

742

Figure 1.

743
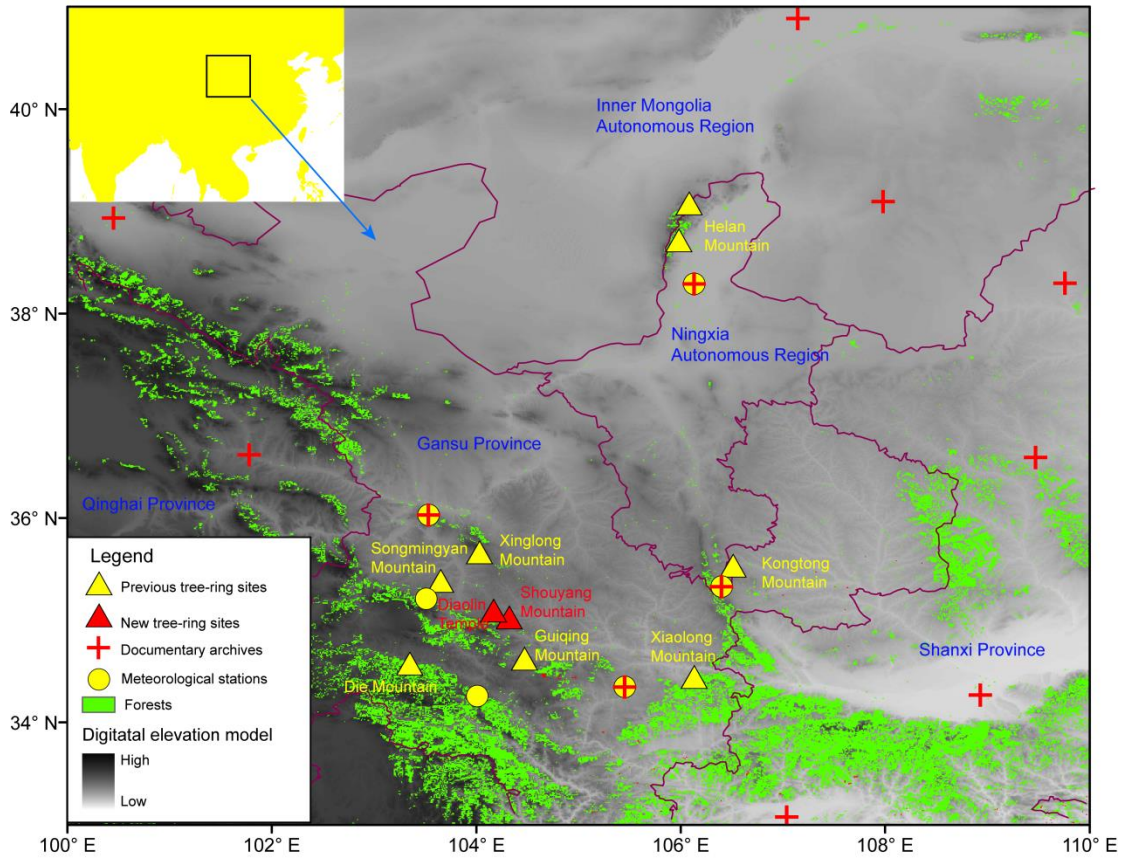
744

745

746

747

748

749

750

751

752

753

754
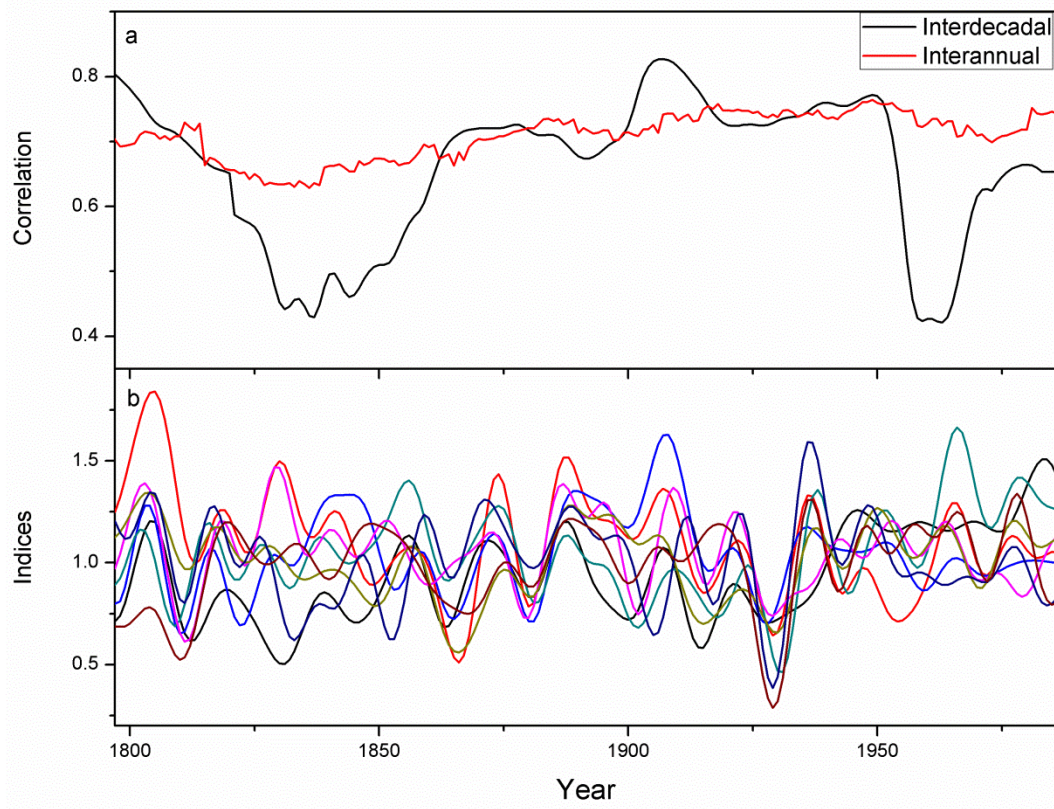
755

756   **Figure 2**.

757

758

759

760

761

762

763

764

765

766

767

768

Figure 3.

769
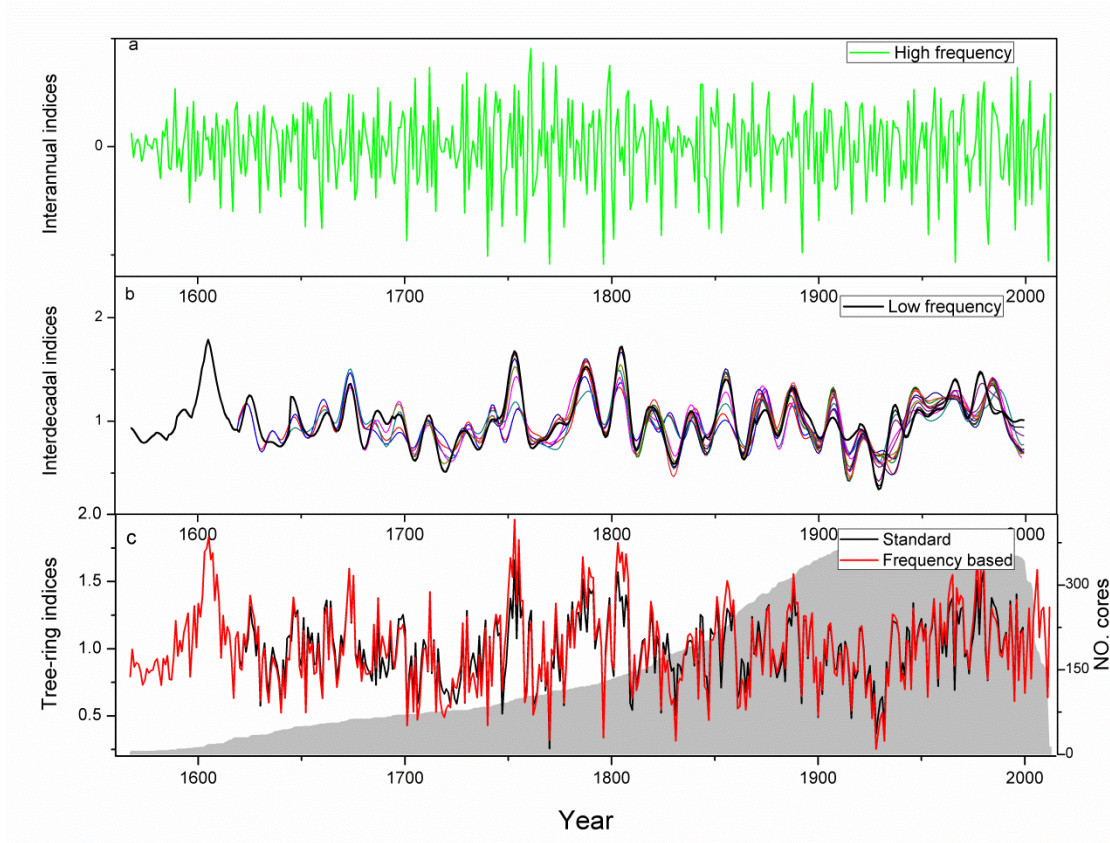
770

771

772

773

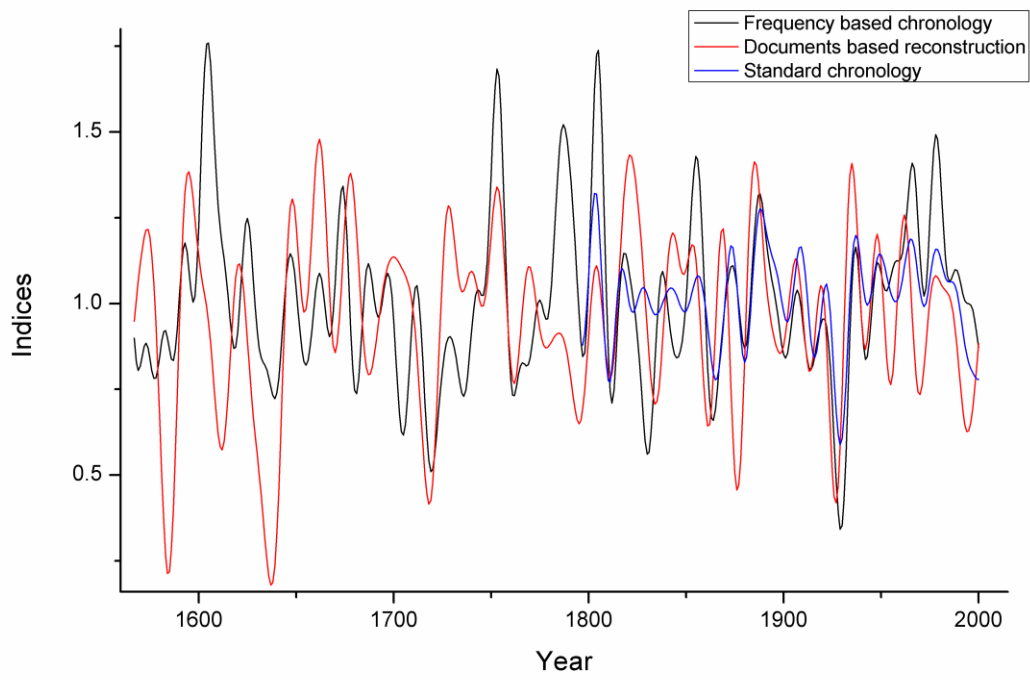774

775

776

777

778

779

780

781

782   **Figure 4**.
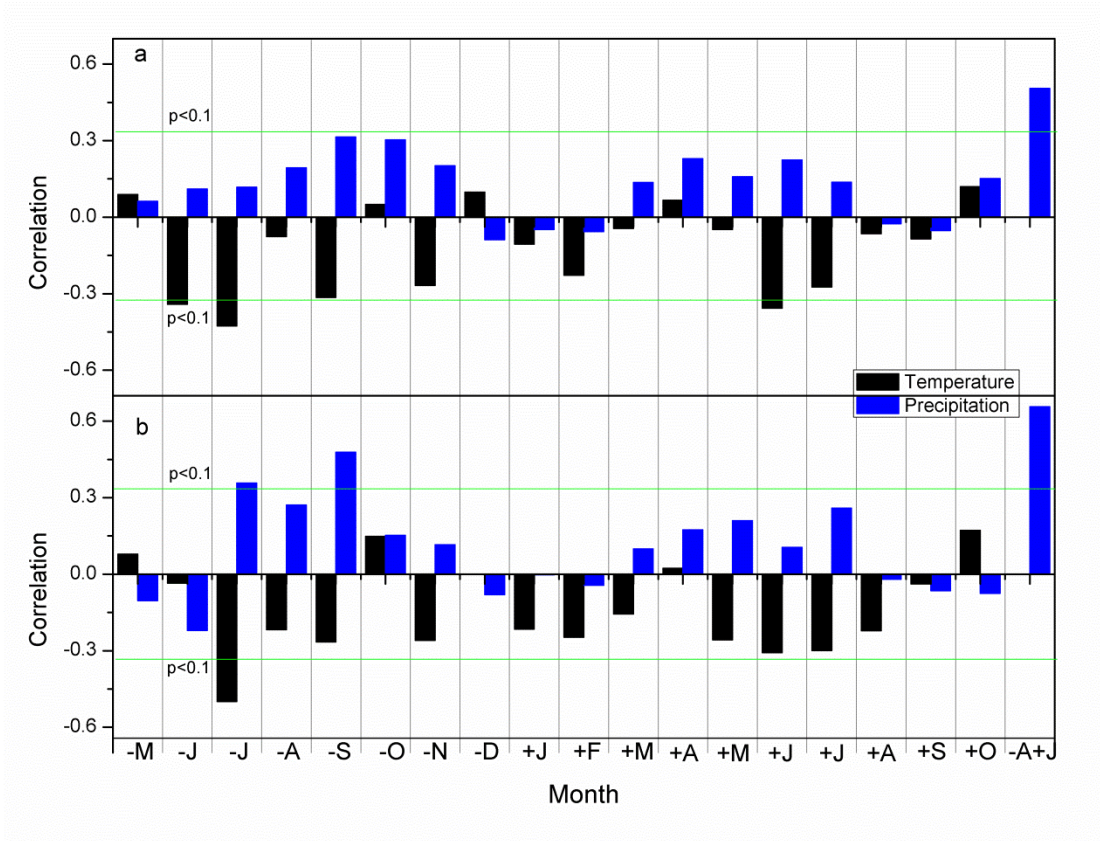
783

784

785

786

787

788

789

790

791

792

793

794
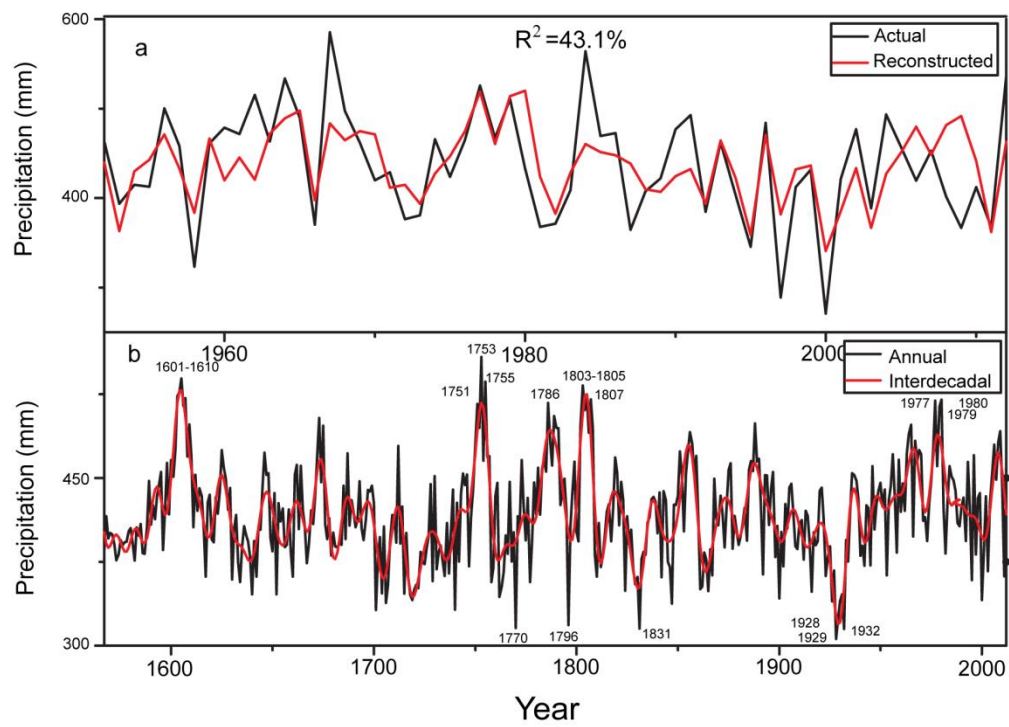
795

796   **Figure 5**.

797

798

799

800

801

802

803

804

805

806

807

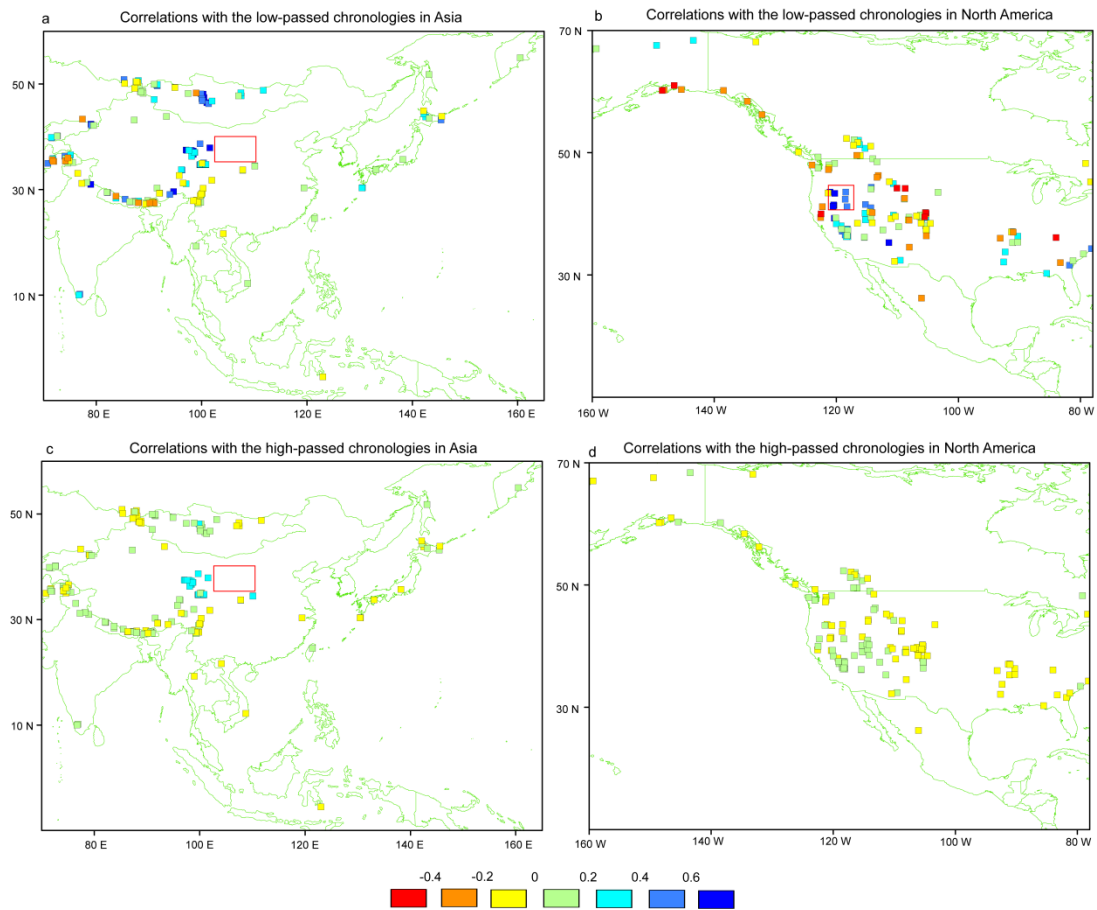808

809 **Figure 6**.

810

811

812

813

814

815

816

817

818

819

820

Figure 7.

833

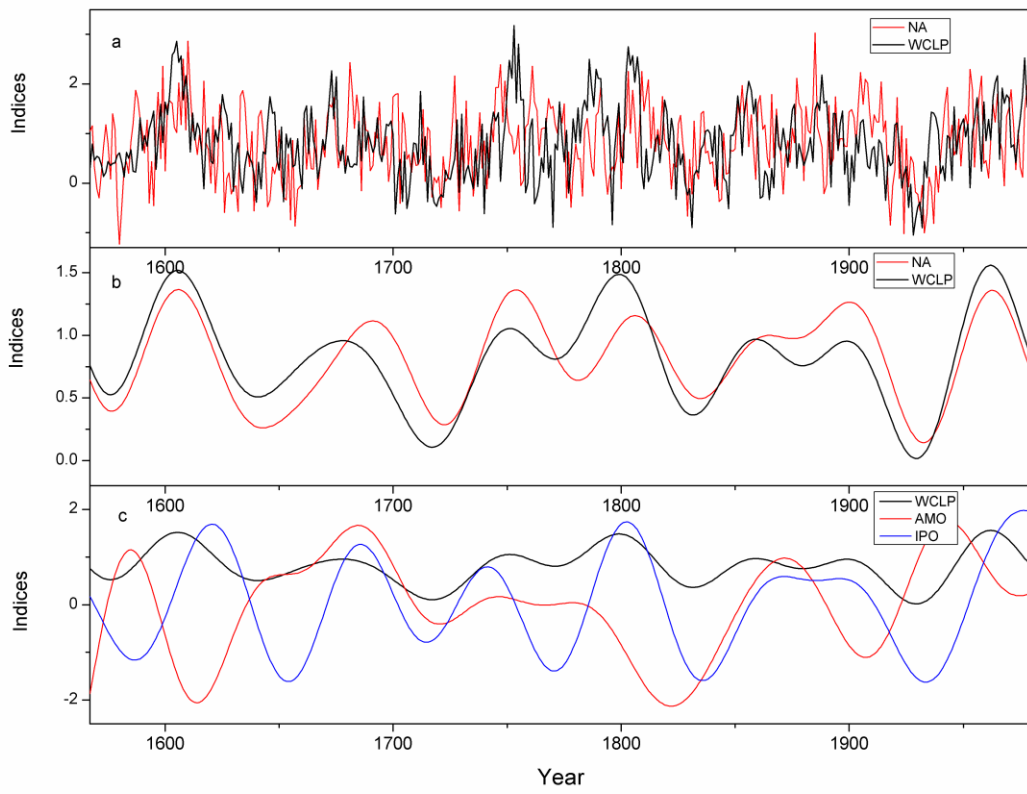**Figure 8**.

835